Rapid Communications | Editors' Suggestion

Approaching the quantum critical point in a highly correlated all-in–all-out antiferromagnet

Yishu Wang,[1,2] T. F. Rosenbaum,[1] D. Prabhakaran,[3] A. T. Boothroyd,[3] and Yejun Feng[1,4,*]

[1]*Division of Physics, Mathematics, and Astronomy, California Institute of Technology, Pasadena, California 91125, USA*

[2]*The Institute for Quantum Matter and Department of Physics and Astronomy, The Johns Hopkins University, Baltimore, Maryland 21218, USA*

[3]*Department of Physics, University of Oxford, Clarendon Laboratory, Oxford OX1 3PU, United Kingdom*

[4]*Okinawa Institute of Science and Technology Graduate University, Onna, Okinawa 904-0495, Japan*

(Received 11 October 2019; revised manuscript received 13 May 2020; accepted 15 May 2020; published 4 June 2020)

Continuous quantum phase transition involving all-in–all-out (AIAO) antiferromagnetic order in strongly spin-orbit-coupled 5*d* compounds could give rise to various exotic electronic phases and strongly-coupled quantum critical phenomena. Here we experimentally trace the AIAO spin order in $Sm_2Ir_2O_7$ using direct resonant x-ray magnetic diffraction techniques under high pressure. The magnetic order is suppressed at a critical pressure $P_c = 6.30$ GPa, while the lattice symmetry remains in the cubic Fd-$3m$ space group across the quantum critical point. Comparing pressure tuning and the chemical series $R_2Ir_2O_7$ reveals that the approach to the AIAO quantum phase transition is characterized by contrasting evolutions of the pyrochlore lattice constant a and the trigonal distortion surrounding individual Ir moments, which affects the 5*d* bandwidth and the Ising anisotropy, respectively. We posit that the opposite effects of pressure and chemical tuning lead to spin fluctuations with different Ising and Heisenberg character in the quantum critical region. Finally, the observed low pressure scale of the AIAO quantum phase transition in $Sm_2Ir_2O_7$ identifies a circumscribed region of P-T space for investigating the putative magnetic Weyl semimetal state.

DOI: 10.1103/PhysRevB.101.220404

The mix of magnetic interactions, electron correlations, and spin-orbit coupling informs the competition between different quantum ground states and ordering mechanisms, ranging from Mott to Slater antiferromagnetic insulators [1,2], phonon to spin-fluctuation-mediated superconductivity [3,4], and Kondo screening to Ruderman-Kittel-Kasuya-Yosida exchange in heavy fermion materials [5]. For 5*d* pyrochlores such as $R_2Ir_2O_7$ (R = Y, Eu, Sm, Nd), the interplay between intermediate electron correlations and strong spin-orbit coupling leads to all-in–all-out (AIAO) antiferromagnetic order and, potentially, nontrivial topological band structure, commonly known as a Weyl semimetal of broken time-reversal symmetry [6–10]. Conversely, without electron correlation, strong spin-orbit coupling could induce a different topological Weyl state of broken inversion symmetry, as proposed in nonmagnetic pyrochlores with a breathing lattice [11].

AIAO spin order exists in a pyrochlore lattice when all spins are aligned along the local (1,1,1) axis either towards (all-in) or away from (all-out) the center of the tetrahedron [6–10,12–17]. In 5*d* pyrochlores, it has been verified experimentally in $R_2Ir_2O_7$ (R = Lu, Yb, Tb, Eu, Sm, Nd) and $Cd_2Os_2O_7$ [12–17]. However, recent angle-resolved photoemission measurements on both magnetic $Nd_2Ir_2O_7$ and nonmagnetic $Pr_2Ir_2O_7$ as the end member of the $R_2Ir_2O_7$ series demonstrate parabolic nodal structures [2,18] that raise questions about the existence of magnetic Weyl semimetal phases in these compounds at ambient pressure. Under suitable tuning processes, such as pressure, exotic states may yet emerge over an adjustable parameter space spanned by the Coulomb interaction U and spin-orbit coupling λ, normalized to the hopping integral t [18,19]. Given that the presence of AIAO magnetic order serves as a gauge of electron correlations, its quantum critical point, where the magnetic order is suppressed to zero at zero temperature, could identify some of the most intriguing regions of intermediate to strong coupling physics in 5*d* compounds [6–10]. For example, it has been suggested that $Pr_2Ir_2O_7$ develops a two-in–two-out spin-ice configuration that melts into a metallic spin liquid at $T < 0.4$ K in the proximity of its AIAO quantum critical point [20].

The iridate pyrochlores $R_2Ir_2O_7$ provide a series of model systems susceptible to continuous tuning, with an approximately local $J_{\text{eff}} = 1/2$ moment from the Ir^{4+} ions of the 5*d* t_{2g} band [15] and a number of germane theoretical calculations [6–10]. $Sm_2Ir_2O_7$, with proven AIAO order [14], negative pressure dependence of its insulating phase [21], and available high-quality single crystals, is a particularly promising experimental choice. Here, using resonant x-ray magnetic diffraction (Refs. [12–14,22–25], Supplemental Material), we demonstrate that the AIAO spin order in $Sm_2Ir_2O_7$ experiences a continuous quantum phase transition at a modest critical pressure $P_c = 6.30$ GPa with preserved lattice space group, exemplifying a directly tracked AIAO quantum critical point in iridates under pressure. Moreover, the pressure evolution of $Sm_2Ir_2O_7$ follows a different pathway across the U/t-λ/t phase space compared with the $R_2Ir_2O_7$ chemical

*yejun@oist.jp

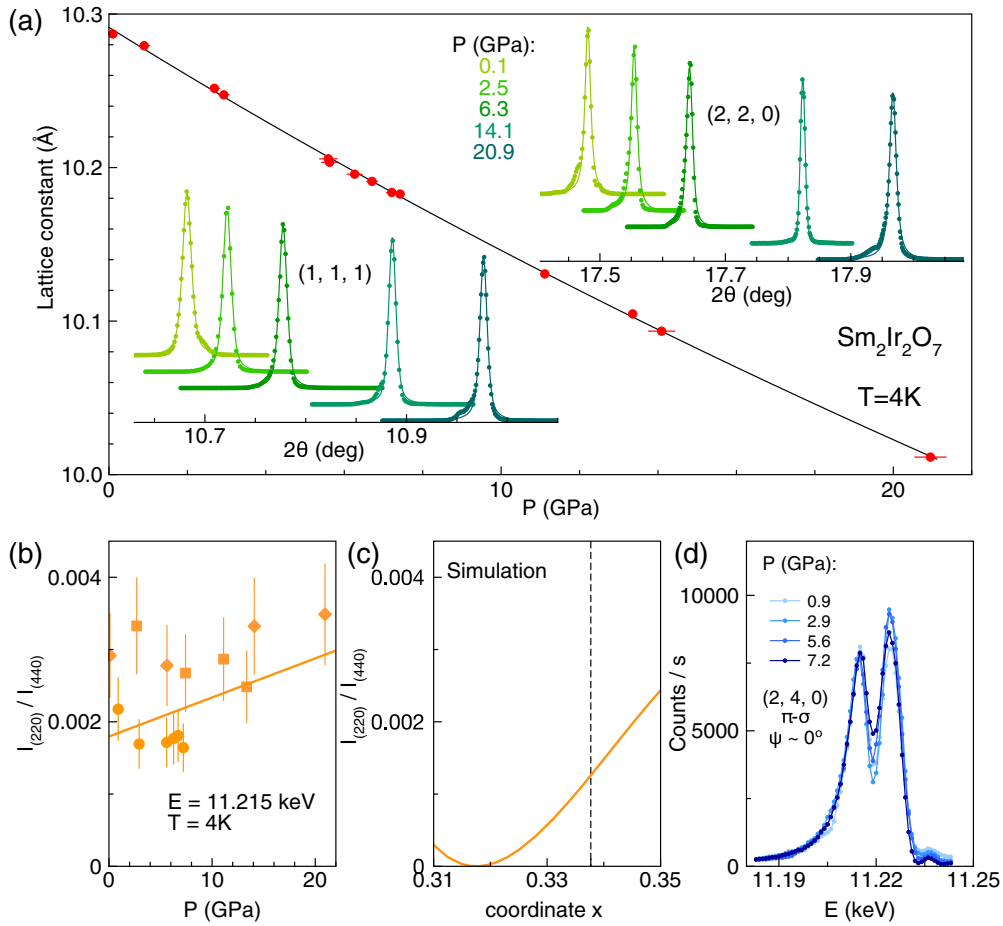

FIG. 1. (a) Lattice constant is fit to a two-parameter Birch equation, with an isothermal bulk modulus $B_0 = 215.6 \pm 4.8$ GPa, and its pressure derivative $B' = 3.9 \pm 0.5$. (Inset) Representative longitudinal (θ-2θ) scans of the (2,2,0) and (1,1,1) reflections showing single peaks with minimal traces of lattice stress. Our measured B' is much smaller than that of the silver manometer, in sharp contrast to several accounts of large B' values of iridate pyrochlores in the literature [30]. (b) Diffraction intensities of (2,2,0) reflection normalized by those of (4,4,0) reflection as a function of pressure. Different symbols (circle, square, and diamond) in (b) and Figs. 4(a) and 4(b) represent each of three individual samples studied. (c) Simulation of the relative intensity $I_{(220)/(440)}$ as a function of x. (d) The ATS resonance at four pressures and 4 K. The spectral shape has no azimuthal dependence at (2,4,0) and (0,−2,4) reflections with $\psi \sim 0^\circ$ and $\sim 35^\circ$, respectively, up to 21 GPa (not shown). More details are available in Supplemental Material.

series, providing further clues to the nature of intermediate to strong coupling physics in this model system.

The pyrochlore structure in the Fd-3m space group is fully characterized by two parameters, the lattice constant a and the coordinate parameter x [9]. From the single-peaked (1,1,1) and (2,2,0) diffraction profiles, $Sm_2Ir_2O_7$ remains in a cubic structure to at least 21 GPa, and the lattice constant $a(P)$ evolves continuously at 4 K without any visible sign of a phase transition (Fig. 1). The simple lattice evolution strongly suggests a continuous AIAO quantum phase transition, motivating a full polarization analysis of resonantly scattered x-ray diffraction signals, in pursuit of the most unambiguous and comprehensive understanding of lattice, orbital, and magnetic behavior (Figs. 2–4, Supplemental Material, Refs. [12–14,22,24,25]). The cubic space group under pressure is illustrated by measured (0,0,6) and (0,−2,4) diffraction intensities in the polarization-preserving π-π' channel, which are minimal and constant at 6×10^{-6} level of the main (0,0,4) reflection through 21 GPa [Fig. 4(b)]. This rules out F4-3m and $F4_132$ as the potential high-pressure space group, and the Fd-3m space group likely persists at 4 K to 21 GPa. The exclusion of these two space groups, especially a breathing lattice instability of the F-43m type as observed in $Cd_2Os_2O_7$ [24], indicates that a potential Weyl semimetal state would unlikely be of a broken inversion-symmetry type.

The coordinate parameter x varies from 0.3125 to 0.375, with the limits indicating whether the oxygen atoms on the 48f sites form a perfect octahedron surrounding the Ir site or a perfect cube surrounding the R site of $R_2Ir_2O_7$, respectively. Within the Fd-3 m space group, both Sm and Ir ions in $Sm_2Ir_2O_7$ do not contribute to diffraction intensity of the (2,2,0) reflection. Instead, this intensity arises solely from oxygen ions, allowing Δx to be measured with high sensitivity [24]. For single crystals under high pressure, where a full structure refinement is not practical due to time and geometry constraints, measurements of the (2,2,0) reflection are especially suitable to reveal the evolution of x [24]. The normalized diffraction intensities increase slightly under pressure [Fig. 1(b)], indicating x varies by $\Delta x \sim 0.008 \pm 0.006$

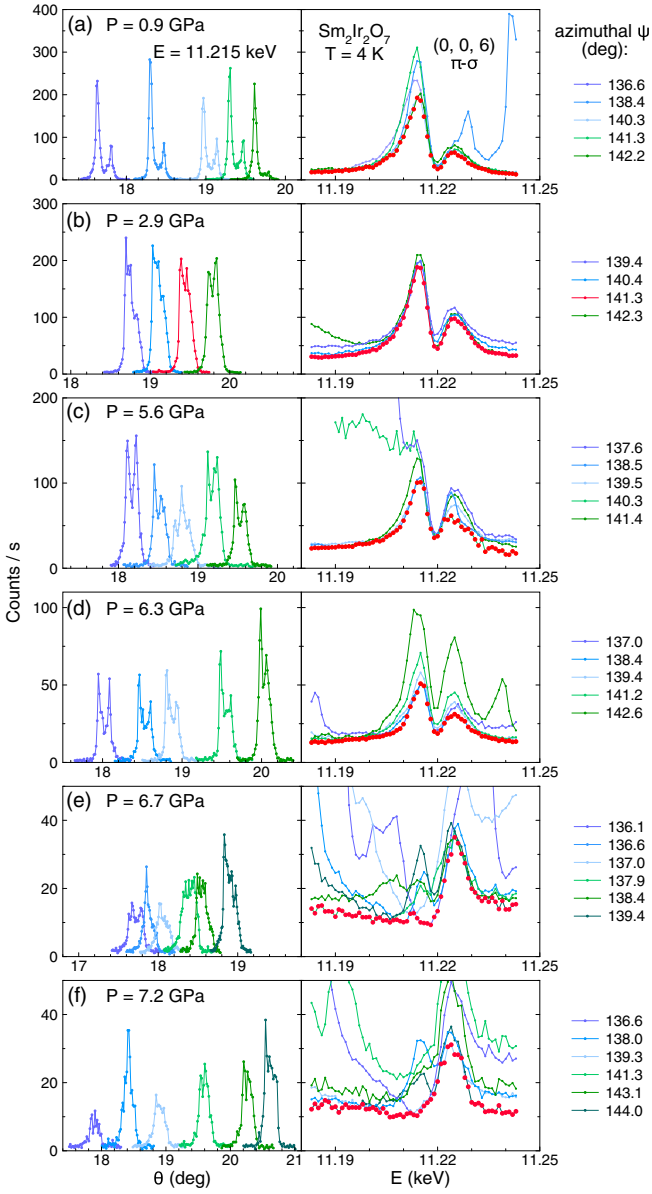

FIG. 2. Raw x-ray magnetic diffraction profiles of both mosaic and energy resonance at (a)–(d) below, and (e), (f) above the critical pressure from one sample. The common spectral weight (marked by solid red circles) between energy spectra at all azimuthal angles, defines the resonance profile. All counting rates are normalized to a 100 mA synchrotron ring current in this figure and Fig. 3.

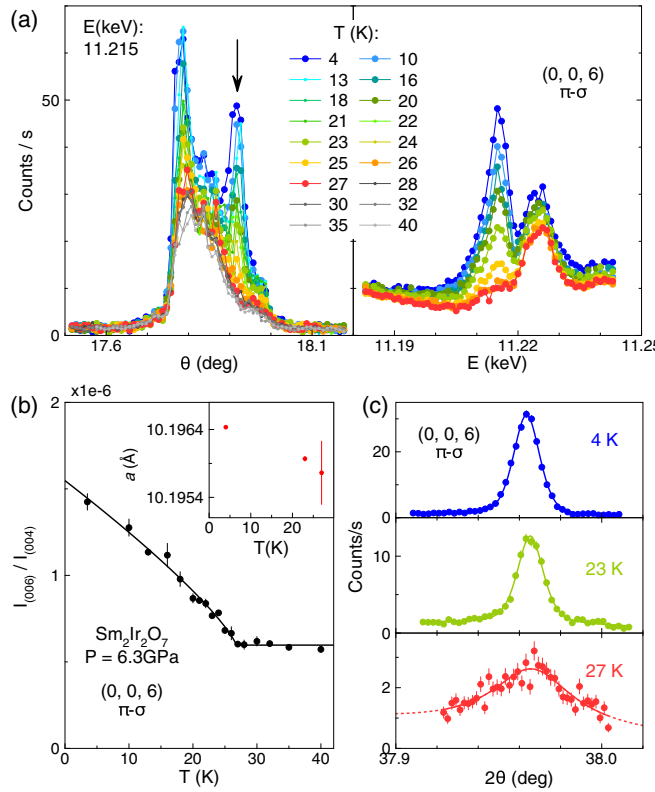

FIG. 3. Temperature evolution of the resonant x-ray magnetic diffraction at 6.26 GPa. (a) Mosaic scans and energy profiles measured at the mosaic position indicated by the arrow. Above 27 K, the magnetic resonance below the Ir L_3 edge [13] fully disappears and the mosaic profile no longer varies. Given the similar shapes of three mosaic profiles at azimuthal $\psi = 137^\circ \sim 140^\circ$ in Fig. 2(d), the residual mosaic form is likely due to dislocations and voids, instead of multiple scattering. For resonance profiles, the residual spectral weight above T_N at 11.225 keV is due to enhanced multiple scattering above the absorption edge. (b) Integrated mosaic intensity in (a) vs. temperature, fit to a power law plus a constant. (Inset) Lattice expansion at low temperature demonstrates a noticeable magnetostriction effect. (c) Longitudinal scans of the (0,0,6) reflection, fit to resolution-limited pseudo-Voigt line shapes at 4 and 23 K, and a Lorentzian shape plus a linear background at 27 K.

from ambient pressure to 21 GPa when the change of intensity is compared to simulations [Fig. 1(c)].

The anisotropic tensor susceptibility (ATS) resonance [12–14,22,24] is sensitive to the individual t_{2g} and e_g bands of Ir 5*d* states. Measured at the (2, 4, 0) reflection in the polarization-switching π-σ channel [Fig. 1(d)], the ATS resonance demonstrates a constant shape under pressure. In $R_2Ir_2O_7$, the ATS resonance profile differs in shape from that of the magnetic resonance (Fig. 2 and Refs. [13,14]), indicating that the magnetic electrons are confined in the lower t_{2g} band. Our result in Fig. 1(d) demonstrates that both bands experience no significant energy shift over this pressure range. A constant ATS resonance is also observed in $Cd_2Os_2O_7$ under pressure [24].

Through many resonant x-ray diffraction studies in the recent decade [12–14,22,24], it has been clarified that the magnetic order parameter of the AIAO type of antiferromagnetism can be extracted from the (0,0,6) reflection intensity in a polarization-switching channel under specific azimuthal conditions that would totally suppress the ATS contribution (Supplemental Material [25]). Both the sample mosaic and energy resonance of the (0,0,6) reflection were followed at 4 K across the magnetic quantum phase transition (Fig. 2). Through careful studies of the resonance shapes at finely stepped azimuthal positions, one can distinguish the influence of multiple scattering, extract the true magnetic behavior, and verify the magnetic phase boundary. The effort of minimizing the multiple scattering during the measurement time further

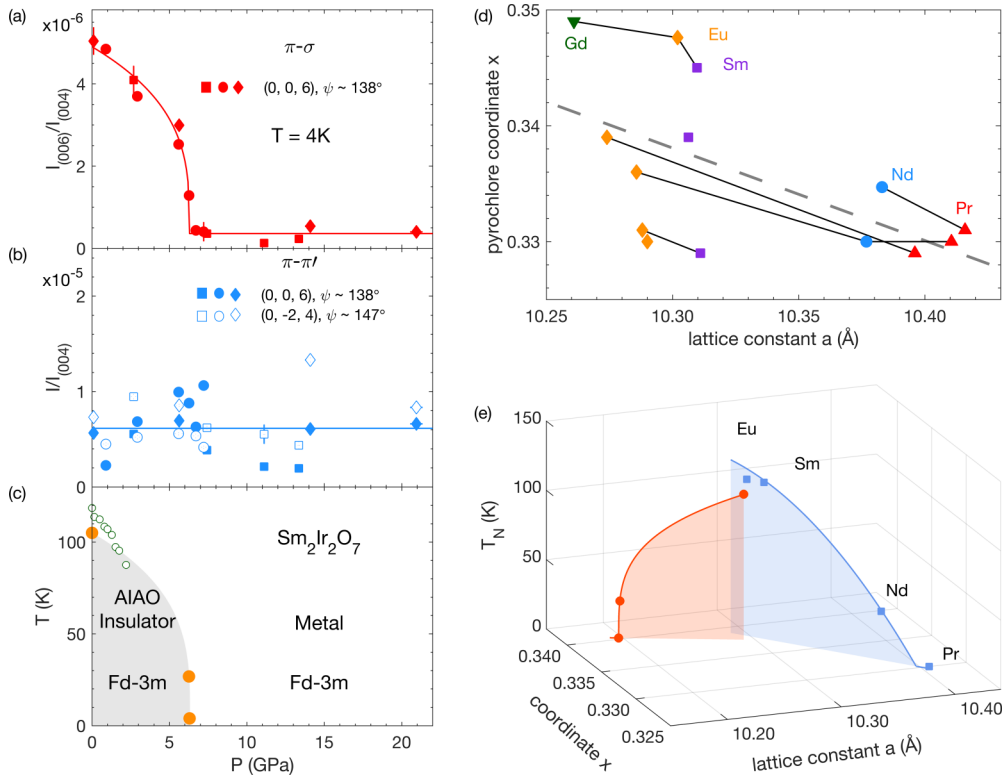

FIG. 4. (a) Integrated magnetic (0,0,6) reflection intensity in the π-σ channel, normalized by the (0,0,4) reflection intensity in the π-π' channel. A power-law fit plus a constant (solid line) reveals $P_c = 6.30$ GPa at $T = 4.0 \pm 0.3$ K. (b) Integrated (0,−2,4) and (0,0,6) reflection intensities in the π-π' channel, normalized by the (0,0,4) reflection intensity, indicate the Fd-$3m$ space group persists to 21 GPa. (c) The projected AIAO phase of $Sm_2Ir_2O_7$ (gray area) is scaled from the power-law fit of the magnetic intensity in (a), with magnetic P-T phase boundary points measured on our samples (orange circles), and metal-insulator transition points (green circles) from Ref. [21]. (d) Correlation between pyrochlore lattice parameters x and a in $R_2Ir_2O_7$ for elements R = Gd (green down triangles), Eu (orange diamonds), Sm (purple squares), Nd (blue circles), and Pr (red up triangles), from seven independent research groups (Supplemental Table, Refs. [21,25,26,31,34–37]). (x, a) values of the same group but of different element R are connected by linear segments, highlighting the correlation between x and a (gray dashed line) despite systematic variations between different crystal growers. (e) Evolution of the AIAO order in the three-dimensional T-a-x phase space as a function of P and R, including $Sm_2Ir_2O_7$ under pressure (red circles) and the R series (blue squares) following the x-a correlation in (d). The opposing branches of doping and pressure point to the different role played by correlations.

allows a detailed study of the temperature evolution of the magnetic (0,0,6) reflection in $Sm_2Ir_2O_7$ at a fixed azimuthal position. At $P = 6.26$ GPa, just below P_c, the mosaic profile is measured from 4 to 40 K, with the energy resonance profile measured at selected temperatures in between [Fig. 3(a)]. The integrated diffraction intensity continuously approaches a constant beyond 27 K [Fig. 3(b)], demonstrating a second-order thermal AIAO phase transition at 6.26 GPa.

High-resolution longitudinal scans of the (0,0,6) reflection at 6.26 GPa and both 4 and 23 K indicate that $Sm_2Ir_2O_7$ still has long-range AIAO order, as the diffraction line shapes are instrument resolution limited with a spin correlation length of at least 1450 Å. At 27 K, the line shape broadens to a diffusive shape, indicating a shortened spin correlation length of ∼450 Å at the magnetic transition. Furthermore, our high-resolution 2θ value of the (0,0,6) diffraction reveals that the lattice constant shrinks with increasing temperature from 4 to 27 K due to a decreasing staggered moment $\langle M \rangle$ [Fig. 3(b), inset]. This anomalous $a(T)$ reflects the overall magnetostriction, which was also observed in antiferromagnetic $Nd_2Ir_2O_7$ and NiS_2 at ambient pressure [26,27]. As $a(T)$ evolves similarly to the diffraction intensity in Fig. 3(b), there is a consistent relationship of $\Delta a(T) \sim I_{(006)}(T) \sim \langle M \rangle^2$. The magnetostriction $\Delta a/a \sim 5 \times 10^{-4}$ in $Sm_2Ir_2O_7$ ($T_N = 26.8$ K) is comparable in size to that in $Nd_2Ir_2O_7$ ($T_N = 33$ K) [26]. At $P = 6.7$ GPa, above P_c, there is no observed magnetic resonance [Fig. 2(d)], and a similar study of the mosaic profile generates no temperature dependence up to 20 K.

We fit both the thermal and pressure evolution [Fig. 3(b) and Fig. 4(a)] of the resonant magnetic diffraction intensity to critical power-law forms: $I_{(006)} \sim (T_c\text{-}T)^{2\beta}$ and $I_{(006)} \sim (P_c\text{-}P)^{2\gamma}$. We find $T_c = 26.8 \pm 0.3$ K and $\beta = 0.41 \pm 0.05$ at $P = 6.26$ GPa, and $P_c = 6.30 \pm 0.05$ GPa and $\gamma = 0.15 \pm 0.03$ at $T = 4.0$ K. The exponent β is between the mean-field expectation of 0.5 and three-dimensional Heisenberg spin fluctuations of 0.37, but the order parameter evolves more rapidly under pressure with a small γ.

For the P-T phase diagram of AIAO order in $Sm_2Ir_2O_7$, we scale $T_N(P)$ by the magnetic diffraction intensity $I_{(006)}$ in

Fig. 4(a). This mapping of magnetic intensity to the phase boundary is justified by the consideration that within this small pressure range ($\Delta a \sim 0.10$ Å or $\Delta a/a \sim 1.0\%$), the order parameter $\langle M \rangle$ should connect to the energy scale of T_N as $I_{(006)}(P) \sim \langle M \rangle^2 \sim T_N(P)$, similarly demonstrated in several antiferromagnets under pressure [4,24]. The projected phase boundary $T_N(P)$ is consistent with the three observed phase points [Fig. 4(c)], identified through magnetization $M(T)$ at ambient P, the temperature dependence of $I_{(006)}(T)$ at $P = 6.26$ GPa, and the pressure dependence of $I_{(006)}(P)$ at $T = 4$ K. At ambient pressure, Sm moments in $Sm_2Ir_2O_7$ have an estimated size of $0.1\,\mu_B/Sm^{3+}$, and order at $T \sim 10$ K [28]. Both are much smaller than the Ir moment size of $0.3\,\mu_B/Ir^{4+}$ and the ordering temperature $T_N \sim 110$ K [28]. By comparison to several pyrochlore iridates with large A-site moments ($2.6 - 9\,\mu_B$ per Nd^{3+}, Er^{3+}, or Tb^{3+}) [29,30], the magnetic coupling strength between Sm^{3+} $4f$ moments is likely much below 0.1 meV [29], and Sm^{3+} ordering relies on the assistance of the Ir^{4+} molecular field, making it parasitic to the Ir AIAO order. We thus consider Sm^{3+} ions as disordered at $P_c = 6.30$ GPa.

Although both pressure and chemical variation of R (from Eu to Pr) in $R_2Ir_2O_7$ [19] are effective in suppressing T_N to zero while the lattice persists in the cubic Fd-$3m$ symmetry, there exist microscopic differences between these two tuning mechanisms. For the two structural parameters a and x of the pyrochlore lattice, a decreases ~1.0% at P_c in $Sm_2Ir_2O_7$, but increases ~1.5% in the chemical series from Eu to Pr [Fig. 4(d)]. The parameter x indicates compressive trigonal distortion of the octahedron IrO_6. For $Eu_2Ir_2O_7$ and $Pr_2Ir_2O_7$ at ambient pressure, x reduces from 0.339 to 0.330 [Fig. 4(d)]. However, x increases by $\sim 0.0025 \pm 0.0017$ in $Sm_2Ir_2O_7$ at P_c (Fig. 1). In other $5d$ AIAO pyrochlores, x increases from 0.330 to 0.335 in $Eu_2Ir_2O_7$ over 17 GPa at 295 K [31], and from 0.319 to about 0.325 in $Cd_2Os_2O_7$ over 40 GPa at 4 K [24].

AIAO order exists in pyrochlore lattices due to both the electron correlation, U/t, and local Ising spin anisotropy. From symmetry considerations, the pyrochlore structure naturally hosts the Dzyaloshinskii-Moriya (DM) interaction, and the *direct* DM interaction leads to the AIAO order [32]. As the DM strength is proportional to the spin-orbit coupling λ, AIAO order has been discovered in many $5d$ pyrochlores. The trigonal distortion of local crystal fields is of similar strength to λ [14,33], and varies the Ir-O-Ir bond angle to affect all ranks of the superexchange interaction. The increasing x in the chemical series sharpens the Ir-O-Ir bond angle from $\sim 131.3^\circ$ at $x = 0.330$ in $Pr_2Ir_2O_7$ to $\sim 126.7^\circ$ at $x = 0.339$ in $Eu_2Ir_2O_7$. By contrast, a shrinking $a(P)$ directly increases the $5d$ bandwidth or equivalently the hopping strength t. A 3% volume reduction at 6.7 GPa would inject ~600 meV energy into each unit cell [22], presumably distributed among all valence electrons at the Fermi surface, with half to broaden the Ir $5d$ band. The increased spatial extent of Ir $5d$ orbitals under pressure reduces U/t. Conversely, the lattice expansion in the chemical series $R_2Ir_2O_7$ reduces the hopping strength t towards the paramagnetic metal. We thus expect t to be predominantly affected by a, while the spin anisotropy is controlled by x.

The contrasting effects of pressure and chemical tuning now become clear and are captured in Fig. 4(e). Pressure maintains the axial nature of the local spin anisotropy, but increases the hopping integral t and reduces U to suppress the long-range order. Chemical tuning of $R_2Ir_2O_7$ suppresses the AIAO state by reducing the axial spin anisotropy towards a more isotropic Heisenberg state, mainly through a weakened DM interaction from a more obtuse Ir-O-Ir angle [7,10]. There are likely two separate pathways across the quantum phase boundary in U/t-λ/t parameter space [Fig. 4(e)] [19], accompanied by different types of spin fluctuations at the respective critical points.

A metal-insulator transition runs concurrently with the AIAO magnetic order in $R_2Ir_2O_7$ ($R =$ Eu, Sm, and Nd) at ambient pressure, and was measured in pelleted polycrystalline $Sm_2Ir_2O_7$ up to 2.2 GPa [21]. It demonstrates a negative pressure dependence similar to our measured AIAO magnetic phase boundary [Fig. 4(c)]. Several theoretical simulations [6,7,9] have suggested the existence of a Weyl semimetallic AIAO phase between the AIAO Mott insulator and the paramagnetic metal. While the Coulomb interaction U varies from 0.5 to 2 eV in various models, there seems to be agreement that the Weyl semimetal phase spans a finite width of $\Delta U \sim 0.2$ eV. As the pressure-driven AIAO quantum phase transition happens within ~0.3 eV change in t from the ambient condition, a span of $\Delta U \sim 0.2$ eV would likely cover the whole pressure range of AIAO order evolution in $Sm_2Ir_2O_7$. Nevertheless, given the small critical exponent γ and the strongly convex shape of the P-T phase diagram, the electronic structure might well only demonstrate topological features very close to the pressure phase boundary (if at all). Our direct magnetic phase diagram pinpoints such a narrow phase space of interest.

$Sm_2Ir_2O_7$ represents one of the cleanest systems to explore the AIAO type of antiferromagnetic quantum criticality with large Ir moments maintaining local Ising anisotropy under pressure. With no breaking of inversion symmetry through the quantum critical point, it provides a fascinating comparison to the strongly coupled AIAO quantum phase transition in $Cd_2Os_2O_7$ [24]. Although the electronic evolution through P_c remains to be resolved, theoretical simulations agree in general that a metallic paramagnetic phase exists beyond the AIAO order. Whether or not there exists a magnetic Weyl semimetal phase, a strong electronic evolution likely exists close to the AIAO quantum critical point, providing the quantum critical region strong-coupling characteristics with intertwined spin and charge fluctuations.

We are grateful to Y. Ren for discussions. Y.F. acknowledges support from Okinawa Institute of Science and Technology Graduate University with subsidy funding from the Cabinet Office, Government of Japan. The work at Caltech was supported by National Science Foundation Grant No. DMR-1606858. The work in Oxford was supported by U.K. Engineering and Physical Sciences Research Council Grant No. EP/N034872/1. The work at the Advanced Photon Source of Argonne National Laboratory was supported by the U.S. Department of Energy Basic Energy Sciences under Contract No. DE-AC02-06CH11357.

[1] R. Arita, J. Kunes, A. V. Kozhevnikov, A. G. Eguiluz, and M. Imada, Phys. Rev. Lett. **108**, 086403 (2012).

[2] M. Nakayama, T. Kondo, Z. Tian, J. J. Ishikawa, M. Halim, C. Bareille, W. Malaeb, K. Kuroda, T. Tomita, S. Ideta, K. Tanaka, M. Matsunami, S. Kimura, N. Inami, K. Ono, H. Kumigashira, L. Balents, S. Nakatsuji, and S. Shin, Phys. Rev. Lett. **117**, 056403 (2016).

[3] P. Monthoux, D. Pines, and G. G. Lonzarich, Nature (London) **450**, 1177 (2005).

[4] Y. Wang, Y. Feng, J.-G. Cheng, W. Wu, J. L. Luo, and T. F. Rosenbaum, Nat. Commun. **7**, 13037 (2016).

[5] S. Doniach, Physica B+C **91**, 231 (1977).

[6] X. Wan, A. M. Turner, A. Vishwanath, and S. Y. Savrasov, Phys. Rev. B **83**, 205101 (2011).

[7] W. Witczak-Krempa and Y. B. Kim, Phys. Rev. B **85**, 045124 (2012).

[8] L. Savary, E.-G. Moon, and L. Balents, Phys. Rev. X **4**, 041027 (2014).

[9] F. Ishii, Y. P. Mizuta, T. Kato, T. Ozaki, H. Weng, and S. Onoda, J. Phys. Soc. Jpn. **84**, 073703 (2015).

[10] Y. Yamaji and M. Imada, Phys. Rev. B **93**, 195146 (2016).

[11] T. Bzdusek, A. Rüegg, and M. Sigrist, Phys. Rev. B **91**, 165105 (2015).

[12] J. Yamaura, K. Ohgushi, H. Ohsumi, T. Hasegawa, I. Yamauchi, K. Sugimoto, S. Takeshita, A. Tokuda, M. Takata, M. Udagawa, M. Takigawa, H. Harima, T. Arima, and Z. Hiroi, Phys. Rev. Lett. **108**, 247205 (2012).

[13] H. Sagayama, D. Uematsu, T. Arima, K. Sugimoto, J. J. Ishikawa, E. O'Farrell, and S. Nakatsuji, Phys. Rev. B **87**, 100403(R) (2013).

[14] C. Donnerer, M. C. Rahn, M. M. Sala, J. G. Vale, D. Pincini, J. Strempfer, M. Krisch, D. Prabhakaran, A. T. Boothroyd, and D. F. McMorrow, Phys. Rev. Lett. **117**, 037201 (2016).

[15] H. Guo, C. Ritter, and A. C. Komarek, Phys. Rev. B **94**, 161102(R) (2016).

[16] H. Guo, C. Ritter, and A. C. Komarek, Phys. Rev. B **96**, 144415 (2017).

[17] H. Jacobsen, C. D. Dashwood, E. Lhotel, D. Khalyavin, P. Manuel, R. Stewart, D. Prabhakaran, D. F. McMorrow, and A. T. Boothroyd, Phys. Rev. B **101**, 104404 (2020).

[18] K. Kondo, M. Nakayama, R. Chen, J. J. Ishikawa, E.-G. Moon, T. Yamamoto, Y. Ota, W. Malaeb, H. Kanai, Y. Nakashima, Y. Ishida, R. Yoshida, H. Yamamoto, M. Matsunami, S. Kimura, N. Inami, K. Ono, H. Kumigashira, S. Nakatsuji, L. Balents, and S. Shin, Nat. Commun. **6**, 10042 (2015).

[19] W. Witczak-Krempa, G. Chen, Y. B. Kim, and L. Balents, Annu. Rev. Condens. Matter Phys. **5**, 57 (2014).

[20] Y. Tokiwa, J. J. Ishikawa, S. Nakatsuji, and P. Gegenwart, Nat. Mater. **13**, 356 (2014).

[21] W. Liu, H. Han, L. Ma, L. Pi, L. Zhang, and Y. Zhang, J. Alloys Compd. **741**, 182 (2018).

[22] Y. Wang, T. F. Rosenbaum, and Y. Feng, IUCrJ **6**, 507 (2019).

[23] Y. Feng, R. Jaramillo, J. Wang, Y. Ren, and T. F. Rosenbaum, Rev. Sci. Instrum. **81**, 041301 (2010).

[24] Y. Wang, T. F. Rosenbaum, A. Palmer, Y. Ren, J.-W. Kim, D. Mandrus, and Y. Feng, Nat. Commun. **9**, 2953 (2018).

[25] See Supplemental Material at http://link.aps.org/supplemental/10.1103/PhysRevB.101.220404 for detailed information of x-ray diffraction setup at beamline 4-ID-D of the Advanced Photon Source, sample environment, symmetry considerations, pressure calibration, and also tabulated references of the literature data in Fig. 4(d).

[26] H. Takatsu, K. Watanabe, K. Goto, and H. Kadowaki, Phys. Rev. B **90**, 235110 (2014).

[27] Y. Feng, R. Jaramillo, A. Banerjee, J. M. Honig, and T. F. Rosenbaum, Phys. Rev. B **83**, 035106 (2011).

[28] R. Asih, N. Adam, S. S. Mohd-Tajudin, D. P. Sari1, K. Matsuhira, H. Guo, M. Wakeshima, Y. Hinatsu, T. Nakano, Y. Nozue, S. Sulaiman, M. I. Mohamed-Ibrahim, P. K. Biswas, and I. Watanabe, J. Phys. Soc. Jpn. **86**, 024705 (2017).

[29] K. Tomiyasu, K. Matsuhira, K. Iwasa, M. Watahiki, S. Takagi, M. Wakeshima, Y. Hinatsu, M. Yokoyama, K. Ohoyama, and K. Yamada, J. Phys. Soc. Jpn. **81**, 034709 (2012).

[30] E. Lefrançois, V. Simonet, R. Ballou, E. Lhotel, A. Hadj-Azzem, S. Kodjikian, P. Lejay, P. Manuel, D. Khalyavin, and L. C. Chapon, Phys. Rev. Lett. **114**, 247202 (2015).

[31] J. P. Clancy, H. Gretarsson, E. K. H. Lee, D. Tian, J. Kim, M. H. Upton, D. Casa, T. Gog, Z. Islam, B.-G Jeon, K. H. Kim, S. Desgreniers, Y. Baek Kim, S. J. Julian, and Y.-J. Kim, Phys. Rev. B **94**, 024408 (2016).

[32] M. Elhajal, B. Canals, R. Sunyer, and C. Lacroix, Phys. Rev. B **71**, 094420 (2005).

[33] D. Uematsu, H. Sagayama, T.-h. Arima, J. J. Ishikawa, S. Nakatsuji, H. Takagi, M. Yoshida, J. Mizuki, and K. Ishii, Phys. Rev. B **92**, 094405 (2015).

[34] J. N. Millican, R. T. Macaluso, S. Nakatsuji, Y. Machida, Y. Maeno, and J. Y. Chan, Mater. Res. Bull. **42**, 928 (2007).

[35] B. J. Kennedy, Physica B **241–243**, 303 (1998).

[36] N. Taira, M. Wakeshima, and Y. Hinatsu, J. Phys.: Condens. Matter **13**, 5527 (2001).

[37] K. Matsuhira, M. Wakeshima, R. Nakanishi, T. Yamada, A. Nakamura, W. Kawano, S. Takagi, and Y. Hinatsu, J. Phys. Soc. Jpn. **76**, 043706 (2007).